AUT Journal of Electrical Engineering
10.22060/EEJ.2026.25813.6014

A Multiphysics Pressure-Driven Framework for Electrohydraulic Sheet Metal Forming: Numerical Modeling and Formability Evaluation

Ilhem Boutana[1,*], Samir Achouche[2], Bachir Benalia[2]

[1]Associate Professor, Laboratory of Electrical Engineering and Industrial Electronics, Faculty of Science and Technology, University of Jijel, Jijel, 18000, Algeria
[2]Department of Electrical Engineering, University of Jijel, Jijel, 18000, Algeria
[*] Corresponding Author's Email: hafsaoui@univ-jijel.dz

Abstract:

Electrohydraulic Forming is a high-speed forming process that converts electrical energy into mechanical work through an underwater spark discharge, generating a shockwave that deforms a metal sheet into a die. In this paper, we present a numerical model developed in COMSOL Multiphysics to simulate both free forming and die forming of thin sheets. The model treats the electrical discharge as a static pressure applied at the midpoint of the electrodes, replacing the shockwave with a static pressure. Simulations were carried out for *Aluminum*, *Copper*, and *Steel* sheets under varying pressures ($10^4 - 10^5$ Pa). Free-forming results show that displacement increases nearly linearly with pressure, with maximum central deflections of approximately $42mm$ for aluminum, $30mm$ for copper, and $20mm$ for steel at the maximum applied pressure of 10^5 Pa, indicating that aluminum exhibits the highest elastic compliance, followed by copper and steel. It should be noted that these results are obtained within a linear-elastic framework; a complete formability assessment would require the inclusion of plasticity, strain hardening, and strain-rate effects. Die-forming simulations with *conical* and *truncated-conical dies* reveal incomplete die filling, consistent with experimental observations. A *time-dependent analysis using a sinusoidal pressure pulse* demonstrates the transient deformation behavior.

Keywords:

Electrohydraulic Forming, COMSOL Multiphysics, Finite Element Analysis, Sheet Metal Forming, High-Speed Forming

10.22060/EEJ.2026.25813.6014

1. Introduction

High-speed forming processes have attracted considerable interest in the manufacturing sector over the past two decades (e.g., [1-5]), owing to their ability to overcome the formability limits of conventional quasi-static techniques, reduce *springback*, and reproduce *fine die detail*s with a single tool half. Among these processes, *Electrohydraulic Forming* (EHF) stands out for its ability to shape both electrically *conductive* and *non-conductive sheet metals* by converting stored electrical energy into a mechanical shockwave in a liquid medium [6,7].

In EHF, a capacitor bank is discharged through a pair of submerged electrodes, creating a rapidly expanding plasma channel in water. The resulting shockwave and subsequent bubble oscillations impart a high-intensity, short-duration pressure pulse to a nearby workpiece, accelerating it into a one-sided die at velocities exceeding $100\,m/s$ (e.g., [8,9]). Because the deformation occurs in microseconds, the material experiences elevated strain rates, often leading to enhanced formability, sometimes referred to as hyperplasticity, relative to quasi-static stamping [10]. Industrial applications have been demonstrated in the *Automotive*, *Aerospace*, and *Consumer-Goods* sectors (e.g., [11,12]), notably for forming aluminium car-body panels that are difficult to stamp conventionally.

Despite these advantages, the industrial adoption of EHF remains limited. One major obstacle is the difficulty of predicting the process outcome without extensive trial-and-error. The physics is inherently multiphysical, involving high-voltage breakdown, fluid dynamics, phase change, and structural mechanics. Early numerical models attempted to capture the complete fluid–structure interaction using coupled *Eulerian-Lagrangian or ALE* formulations, but these approaches are computationally expensive and require detailed knowledge of the arc characteristics and water thermodynamics (e.g., [13]). A simpler, yet effective, alternative was proposed by Melander *et al.* [14], who replaced the complex hydrodynamic loading with an equivalent static pressure acting on a small zone near the electrode gap. Their finite-element simulations of free and die forming of sheet steels agreed well with experimental bulge profiles and die-filling gaps, demonstrating that a static-pressure idealization can capture the macroscopic deformation for many practical configurations.

Building on this foundational work, recent research on EHF has explored several aspects of the process. Tardif *et al.* [15] investigated the influence of the electrical pulse duration on forming efficiency by modifying the RLC circuit topology to vary the arc discharge regime from underdamped to overdamped, establishing a direct correlation between arc duration and the resulting dome height. Ali *et al.* [16] examined the effect of bridge wire material and diameter on the formability of AA 5754 sheets, complementing experimental measurements of dome height and strain distribution with an alternative finite-element model based on TNT explosives in LSDYNA. A simplified preform design methodology was introduced in [17], targeting cases where even the extended formability of EHF is insufficient to achieve the final shape, thereby enabling the use of high-strength, low-formability alloys in automotive manufacturing. Finally, [18] reported formability tests on dual-phase steels under EHF conditions, noting significantly higher achievable strains compared with quasi-static loading and proposing a modelling technique to analyze the dynamic forming process. However, the existing literature lacks a systematic application of this static-pressure methodology to compare the formability of different lightweight metals under identical EHF conditions. Most published numerical studies focus on a single steel grade or a limited pressure range. Furthermore, the time-dependent response of the sheet to a pulsed pressure, an important aspect for process design, has seldom been simulated in the simplified framework.

1-1- Paper Key Contributions

Following these considerations, the objective of this research is therefore to develop a two-dimensional finite-element model of the EHF process in COMSOL Multiphysics, in which the electric discharge is represented as a uniform static pressure applied at the electrode midpoint, and to apply this model to three engineering metals, aluminum, copper, and structural steel, over a wide range of pressures. The study examines both free forming and forming into conical and truncated-conical dies, and includes a time-dependent analysis using a sinusoidal pressure pulse to capture the inertial response of the sheet. The numerical results are validated against the experimental data to assess the predictive accuracy of the approach. By providing a direct formability comparison and die-filling assessment for three materials, the study aims to offer a rapid, industrially relevant design tool for EHF processes.

1-2- Paper Organization

The remaining part of this paper is organized as follows. Section 2 presents the materials and methods, including the fundamental principles of the EHF model, the governing equations for mechanical equilibrium and material behavior, the material properties of the three metals examined, and the finite element meshing and boundary conditions implemented in COMSOL Multiphysics. Section 3 presents the numerical results and discussion, covering the free-forming analysis of aluminum, a comparative formability assessment of aluminum, copper, and steel, die-forming simulations into conical and truncated-conical dies, and a time-dependent analysis under a sinusoidal pressure pulse. Finally, Section 4 summarizes the main conclusions of this study and outlines directions for future research.

2. Materials and Methods

In this Section, we present our proposed numerical framework developed to simulate EHF, including geometric representation, governing equations, and boundary conditions.

2-1- Fundamental Principles and Model Description

Electrohydraulic forming process, schematically illustrated in Fig. 1, is based on the conversion of stored electrical energy into mechanical work. A large capacitor bank is discharged through a pair of electrodes submerged in a dielectric liquid, typically water. The resulting arc rapidly vaporizes the surrounding fluid, generating a high-pressure shockwave that propagates toward the workpiece. This transient pressure pulse drives the sheet metal blank into a one-sided die, enabling either the formation of a specific shape or free deformation. The process is characterized by extremely short forming times and workpiece velocities exceeding 100 m/s, which can enhance the formability of many metals and reduce springback [9,10].

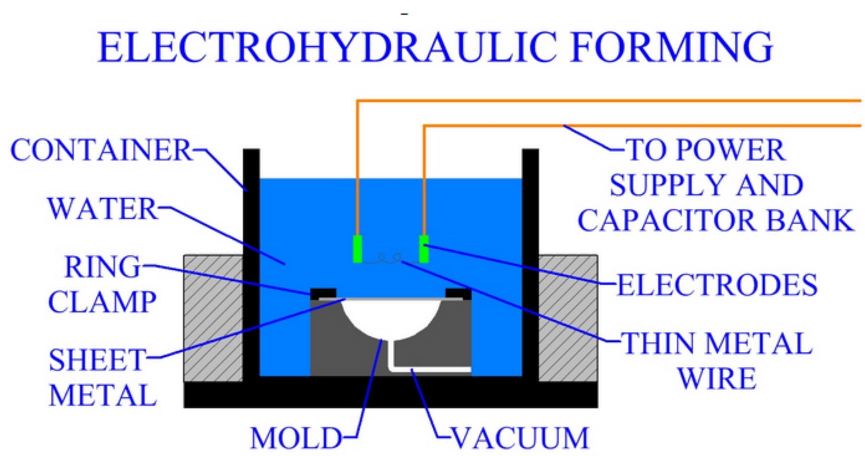

Fig. 1. Schematic View of Electrohydraulic Forming System

To make the numerical simulation of such a complex multiphysics phenomenon tractable for parametric design studies, the present model replaces the entire fluid–structure interaction and electrical discharge physics with an equivalent static pressure load. This approach, originally validated by Melander *et al.* [14] for sheet steels, assumes that the macroscopic deformation pattern is predominantly governed by the peak pressure magnitude and the mechanical stiffness of the blank, and that the spatial and temporal details of the shockwave propagation can be neglected to a first approximation.

Accordingly, the computational domain is reduced to a two-dimensional plane-stress representation of the sheet blank, $200\ mm$ long and $1\ mm$ thick, clamped at both ends (see Fig. 2). A uniform static pressure P is applied on a small segment of length $d = 10\ mm$ at the centre of the upper edge, representing the effect of the spark-generated pressure pulse. The magnitude of P is varied in the range $10^4\ Pa$ to $10^5\ Pa$, covering typical industrial EHF energy densities. The blank material is considered linearly elastic and isotropic. Plastic deformation, thermal effects, and fluid motion are not accounted for in this simplified model.

10.22060/EEJ.2026.25813.6014

It is important to note that the pressure range selected here is intentionally sub-yield for the materials considered, meaning that the applied pressures remain below the elastic limits of the sheet metals.

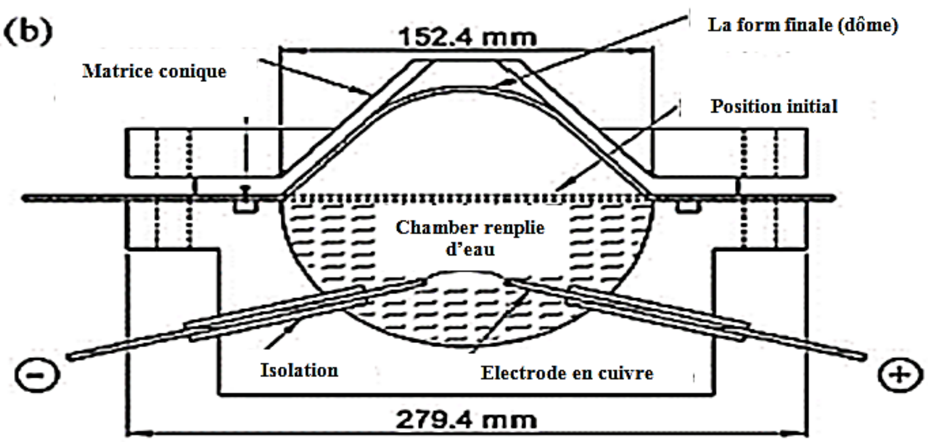

Fig. 2. EHF Experimental Configuration Adapted from [14]

This choice serves two purposes. First, it aligns with the experimental configuration of Melander *et al.* [14], who demonstrated that the macroscopic deformation of sheet metals under EHF loading can be adequately captured by equivalent static pressures within this order of magnitude. Second, and more importantly, the sub-yield range allows the present elastic model to serve as a benchmark for comparing the relative deformation behavior of different materials under identical loading conditions, without the additional complexity introduced by plastic yielding, strain hardening, or strain-rate effects. This approach is consistent with the primary goal of the study: to provide a rapid, industrially relevant design tool for comparing materials and assessing die-filling feasibility, rather than to reproduce exact absolute deformation magnitudes.

2-2- Governing Equations

The sheet blank is modelled as an isotropic, linearly elastic solid undergoing small deformations. Its motion is governed by the fundamental equations of solid mechanics, supplemented by the Navier-Stokes equations for the surrounding fluid.

10.22060/EEJ.2026.25813.6014

2-2-1 Mechanical Equilibrium

The fundamental equation that governs the deformation of any continuous solid is the balance of linear momentum. In three dimensions, and in the absence of body forces, this is expressed by *Newton's second law* (e.g., [19]) applied to a deformable medium:

$$\rho\frac{\partial^2 \boldsymbol{u}}{\partial t^2} - \nabla.\boldsymbol{\sigma} = \vec{F} \tag{1}$$

Where ρ is the mass density of the material, $\boldsymbol{u} = (u, v, w)$ is the displacement vector, and $\boldsymbol{\sigma}$ is the second-order Cauchy stress tensor. In the stationary simulations (i.e., free-forming and die-forming cases), the inertia term is omitted, which reduces Eq. (1) to the following static equilibrium condition:

$$\nabla.\boldsymbol{\sigma} = \vec{F} \tag{2}$$

2-2-2 Strain–Displacement Relationship

Under the assumption of small deformations, the state of strain at a point is fully described by the symmetric part of the displacement gradient. In component form, the strain tensor $\boldsymbol{\varepsilon}$ is written as follows:

$$\varepsilon_{i,j} = \frac{1}{2}\left(\frac{\partial u_i}{\partial x_j} + \frac{\partial u_j}{\partial x_i}\right) \tag{3}$$

Explicitly, the normal and shear components are the following ones:

10.22060/EEJ.2026.25813.6014

$$\begin{cases} \varepsilon_{xx} = \dfrac{\partial u}{\partial x} \\ \varepsilon_{yy} = \dfrac{\partial v}{\partial y} \\ \varepsilon_{zz} = \dfrac{\partial w}{\partial z} \\ \varepsilon_{xy} = \frac{1}{2}\left(\dfrac{\partial u}{\partial y} + \dfrac{\partial v}{\partial x}\right) = \frac{1}{2}\gamma_{xy} \\ \varepsilon_{yz} = \frac{1}{2}\left(\dfrac{\partial v}{\partial z} + \dfrac{\partial w}{\partial y}\right) = \frac{1}{2}\gamma_{yz} \\ \varepsilon_{xz} = \frac{1}{2}\left(\dfrac{\partial u}{\partial z} + \dfrac{\partial w}{\partial x}\right) = \frac{1}{2}\gamma_{xz} \end{cases} \tag{4}$$

The total strain can be additively decomposed into elastic, thermal, and plastic parts:

$$\varepsilon = \varepsilon_{el} + \varepsilon_{th} + \varepsilon_P \tag{5}$$

where the thermal contribution is defined as $\varepsilon_{th} = \alpha\left(T - T_{ref}\right)$ with α the coefficient of thermal expansion and T_{ref} is the reference (ambient) temperature. In the present modelling of EHF, the temperature rise in the sheet is negligible, and plastic yielding is not considered; hence, the total strain reduces to the elastic part ε_{el}.

2-2-3 Stress–Strain Relationship

The stress state inside the solid is described by the symmetric Cauchy stress tensor:

$$\boldsymbol{\sigma} = \begin{bmatrix} \sigma_x & \tau_{xy} & \tau_{xz} \\ \tau_{yx} & \sigma_y & \tau_{yz} \\ \tau_{zx} & \tau_{zy} & \sigma_z \end{bmatrix} \tag{6}$$

Where the shear components satisfy the following condition:

$$\begin{cases} \tau_{xy} = \tau_{yx} \\ \tau_{xz} = \tau_{zx} \\ \tau_{yz} = \tau_{zy} \end{cases} \tag{7}$$

For a linear-elastic isotropic material, the stress is linearly related to the elastic strain through the fourth-order stiffness tensor. In *Voigt notation*, this relation takes the following form:

AUT Journal of Electrical Engineering
10.22060/EEJ.2026.25813.6014

$$\boldsymbol{\sigma} = D\varepsilon_{el} + \boldsymbol{\sigma_0} \tag{8}$$

With the compliance matrix $\boldsymbol{D^{-1}}$, is given by:

$$D^{-1} = \frac{1}{E}\begin{bmatrix} 1 & -v & -v & 0 & 0 & 0 \\ -v & 1 & -v & 0 & 0 & 0 \\ -v & -v & 1 & 0 & 0 & 0 \\ 0 & 0 & 0 & 2(1+v) & 0 & 0 \\ 0 & 0 & 0 & 0 & 2(1+v) & 0 \\ 0 & 0 & 0 & 0 & 0 & 2(1+v) \end{bmatrix} \tag{9}$$

With:

$$\boldsymbol{\sigma} = D_d\left[\begin{bmatrix} \varepsilon_x \\ \varepsilon_y \\ \varepsilon_z \\ \varepsilon_{xy} \\ \varepsilon_{yz} \\ \varepsilon_{xz} \end{bmatrix} - \begin{bmatrix} \varepsilon_{x0} \\ \varepsilon_{y0} \\ \varepsilon_{z0} \\ \varepsilon_{xy0} \\ \varepsilon_{yz0} \\ \varepsilon_{xz0} \end{bmatrix}\right] + \boldsymbol{\sigma_0} \tag{10}$$

Due to the fact that the sheet used in this study is thin compared to its in-plane dimensions, a plane-stress condition ($\sigma_z = \tau_{xz} = \tau_{xz} = 0$) is invoked, which reduces the three-dimensional relations Eq. (8), Eqs. (9), and (10) to the simpler form presented in Eq. (5).

Indeed, the constitutive relations, presented here, form the fundamental material description employed by the *COMSOL Multiphysics Solid Mechanics interface*. In the finite element solution procedure, these equations serve two essential purposes. First, they define the elasticity matrix, which characterizes the material's stiffness response by relating the elastic strain components, computed from the displacement gradients via Eq. (3), to the resulting stresses at each integration point within an element. This matrix contains the material properties (Young's modulus and Poisson's ratio) and ensures that the stress field is consistently computed from the strain field at every point in the sheet.

Second, the solver to assemble the elemental stiffness matrices directly utilizes these stress-strain relationships. The elemental stiffness matrix relates the nodal displacements to the nodal forces for each

10.22060/EEJ.2026.25813.6014

finite element. The global stiffness matrix is then assembled from all elemental contributions, yielding a linear system of equations where the unknown vector is the nodal displacements, and the right-hand side vector is the equivalent nodal forces derived from the applied pressure load defined in Eq. (11). The solver computes the displacement field by solving this system, which directly produces the deformed shapes and deflection magnitudes presented in Section 3.

Under the invoked plane-stress assumption (where the stress components in the thickness direction are neglected), the three-dimensional tensor relations are reduced to their two-dimensional counterparts. This simplification is appropriate for the thin-sheet geometry employed in this study, where the sheet thickness is only one millimeter compared to a length of two hundred millimeters. This reduction significantly decreases computational cost while preserving the essential structural response of the blank under bending-dominated deformation.

Moreover, the equations that govern the movement of any fluid are the equations of conservation of the quantity of motion and the mass conservation equation described by the *Navier-Stokes equations* [20], presented in the following Eq. (11):

$$\begin{cases} \rho(\vec{V}.\overrightarrow{grad})\vec{V} = \vec{F} - \overrightarrow{grad}\,\mathrm{P} + \eta\Delta\vec{V} + \frac{1}{3}\eta\overrightarrow{grad}(div\vec{V}) \\ \mathrm{div}\,\vec{V} = 0 \end{cases} \tag{11}$$

2-2-4 Coupling Strategy

To model the EHF process in its entirety, it is necessary to couple the mechanical equilibrium of the solid sheet with the fluid flow in the surrounding liquid medium. The fluid domain is governed by the *Navier-Stokes equations* presented in Eq. (11), which describe the conservation of momentum and mass for an incompressible Newtonian fluid. The coupling between the fluid and the solid sheet occurs at the fluid-structure interface, where the fluid pressure acts as a traction boundary condition on the sheet surface, while the deformation of the sheet modifies the fluid domain boundaries.

Theoretically, two coupling strategies exist for such fluid-structure interaction problems: weak coupling and strong coupling [21]. In a weakly coupled approach, the fluid and structural equations are solved alternately, with information exchanged at the interface after each separate solution step. This approach is computationally efficient but may suffer from stability issues for problems involving large deformations or strong coupling between the domains. In contrast, a fully coupled (or monolithic) formulation assembles the governing equations of both domains into a single system and solves them simultaneously, which generally offers superior stability and accuracy [21].

In the present research, a strong coupling strategy is conceptually adopted, as the COMSOL Multiphysics environment permits the simultaneous solution of multiple interacting physical equations within a monolithic solver framework. The coupling term between the mechanical and fluid equations is the pressure field generated by the electric discharge at the electrode gap. Under full coupling, the fluid pressure acts as a time- and space-varying traction boundary condition on the sheet surface, while the resulting sheet displacement modifies the fluid domain boundaries. However, to reduce the computational complexity and make extensive parametric studies feasible, the present model replaces the explicit solution of the fluid domain with a simplified representation: the shockwave is idealized as a uniform static pressure P applied directly on a small segment of the sheet surface, as described in Section 2.1. This simplification is justified by the experimental findings of Melander *et al.* [14], who demonstrated that the macroscopic deformation of sheet metals under EHF loading can be adequately captured by equivalent static pressures, without the need for explicit fluid-structure interaction modeling.

The pressure value is selected to match the impulse magnitude typical of the experiments reported in [14], and its spatial distribution is assumed concentrated around the electrode midpoint. The resulting model is thus a fully coupled multiphysics analysis with a prescribed pressure boundary condition. While COMSOL Multiphysics is indeed capable of solving fully coupled fluid-structure interaction problems using the *Navier-Stokes equations* (see Eq. (11)), the present approach deliberately avoids the computational expense

10.22060/EEJ.2026.25813.6014

and complexity of such simulations, enabling rapid parametric studies of pressure magnitude, material properties, and die geometry. This simplification drastically reduces computational effort while still capturing the essential macroscopic deformation response of the blank, as validated by comparison with experimental data in Section 3.5

2-3- Material Properties

Three metals commonly used in lightweight automotive and aerospace structures were selected for the formability comparison: aluminum, copper, and structural steel. Their mechanical properties, Young's modulus, Poisson's ratio, and mass density ρ, are summarized in Table 1. These values are taken from standard material databases and correspond to the isotropic linear-elastic approximation adopted throughout the simulations.

Table 1. Mechanical Properties of the Sheet Materials

Material	Young's Modulus	Poisson's Ratio	Density ρ $[kg/m^3]$
Aluminum	70	0.33	2700
Copper	110	0.35	8700
Steel	200	0.33	7850

Aluminum is a primary candidate for vehicle light-weighting because of its low density and good specific strength; however, its limited quasi-static formability makes it a typical target for high-speed processes such as EHF. Copper, although denser, is of interest for electrical and thermal applications where deep drawing may be required. Structural steel serves as a baseline representing conventional automotive sheet, with higher stiffness and strength but lower formability under quasi-static conditions.

In the present model, all three materials are treated as perfectly elastic, and plasticity and strain-rate effects are neglected. This simplification is justified by the primary goal of the study: to compare the relative formability trends under the same pressure impulse and to assess whether the static-pressure approach can capture the qualitative differences observed experimentally. While plasticity influences the final permanent

10.22060/EEJ.2026.25813.6014

set, the elastic model already provides reliable information on the relative formability ranking and initial bulging stiffness.

2-4- Finite Element Meshing and Boundary Conditions

The finite-element model was implemented in COMSOL Multiphysics using the two-dimensional Solid Mechanics interface under the plane-stress assumption. The geometry of the sheet blank was discretized using unstructured triangular elements, as shown in Fig. 3. A total of 23 022 elements and 12 037 nodes were employed, with a deliberate local refinement around the central pressure-loaded segment to accurately resolve the stress and strain gradients that develop in the vicinity of the applied load. The mesh density was chosen after a preliminary convergence study, which confirmed that further refinement produced negligible changes in the maximum displacement.

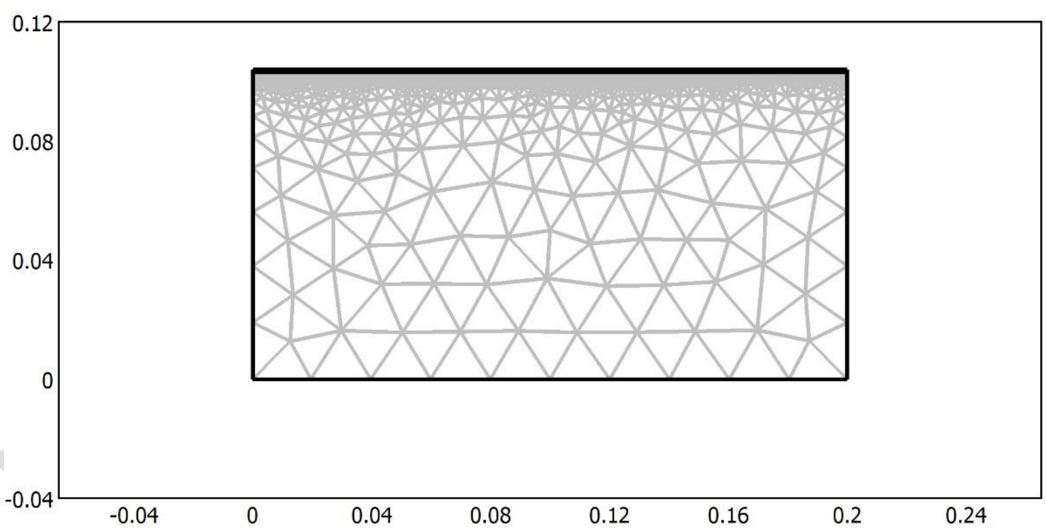

Fig. 3. Finite Element Mesh of the Sheet Blank

The boundary conditions replicate the clamping and loading configuration of the experimental setup [14] and are illustrated schematically in Fig. 2. Specifically:

10.22060/EEJ.2026.25813.6014

(a) The left and right vertical edges of the blank are fully restrained, i.e., all displacement components are set to zero. This condition represents the rigid blank-holder that prevents any movement or rotation of the sheet periphery during the forming event.

$$\boldsymbol{u} = 0 \tag{12}$$

(b) A uniform normal pressure is applied over a small segment of length $d = 10mm$ centered on the upper edge of the blank. This idealized traction substitutes the complex shockwave loading generated by the underwater electric discharge.

$$\boldsymbol{\sigma}.\boldsymbol{n} = -P\boldsymbol{n} \tag{13}$$

(c) The remaining boundaries (the upper edge outside the loaded zone and the entire lower edge) are left traction-free:

$$\boldsymbol{\sigma}.\boldsymbol{n} = 0 \tag{14}$$

3. Results and Discussion

In this Section, we present the numerical results obtained from the free-forming, die-forming, and time-dependent applications and discuss the main findings in light of the experimental data.

3-1- Free-Forming of Aluminum

The free-forming simulations reproduced the EHF setup of Melander *et al.* [14], where a $200\ mm \times 1mm$ sheet was clamped along its short edges and allowed to bulge freely under a pressure pulse without a die. A stationary FEM solver applied a uniform pressure over a central $10\ mm$ region, increasing from $10^4\ Pa$ to $10^5\ Pa$. At low pressure, only minimal deformation occurred due to the sheet's bending stiffness, but increasing pressure produced progressively larger and smoother dome-shaped deflections. The maximum displacement increased from about $7\ mm$ at $2 \times 10^4\ Pa$ to roughly $42\ mm$ at $10^5\ Pa$, with the curvature concentrating near the centre while the sides remained nearly straight (see Fig. 4). The highest predicted displacement agreed well with the experimental free bulging results, confirming that the simplified pressure-based FEM approach can capture the main deformation behavior of EHF free forming. To better

10.22060/EEJ.2026.25813.6014

visualize the overall trend, the deformed mid-lines extracted for all six pressure levels were superimposed in a single graph (see Fig. 5a). It illustrates that the pressure increase not only amplifies the displacement magnitude but also slightly modifies the shape, making the dome steeper without changing its symmetric character. Moreover, a quantitative summary is provided in Fig. 5b, where the maximum vertical displacement u_{max} is plotted as a function of the applied pressure.

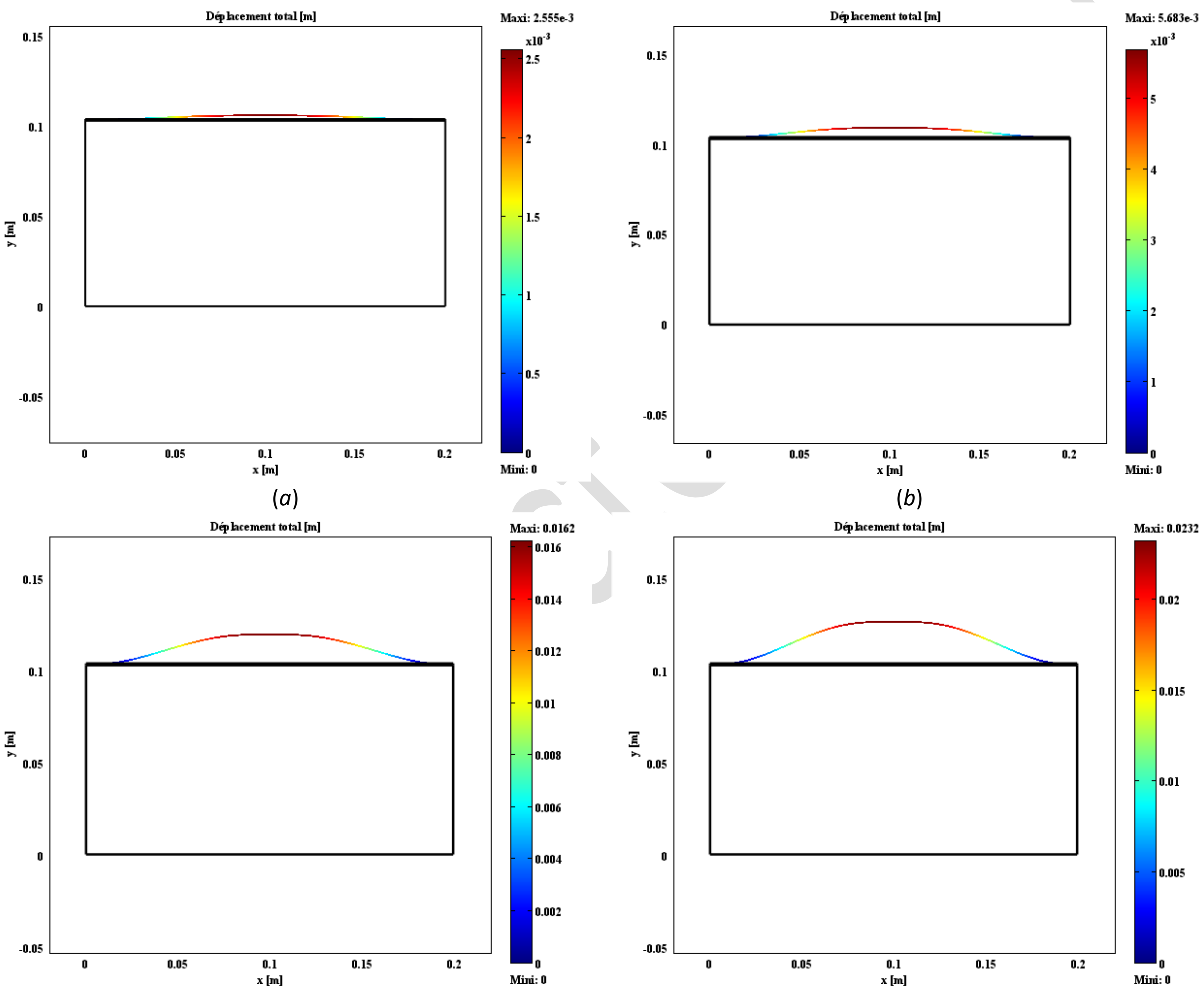

(a) (b)

(c) (d)

10.22060/EEJ.2026.25813.6014

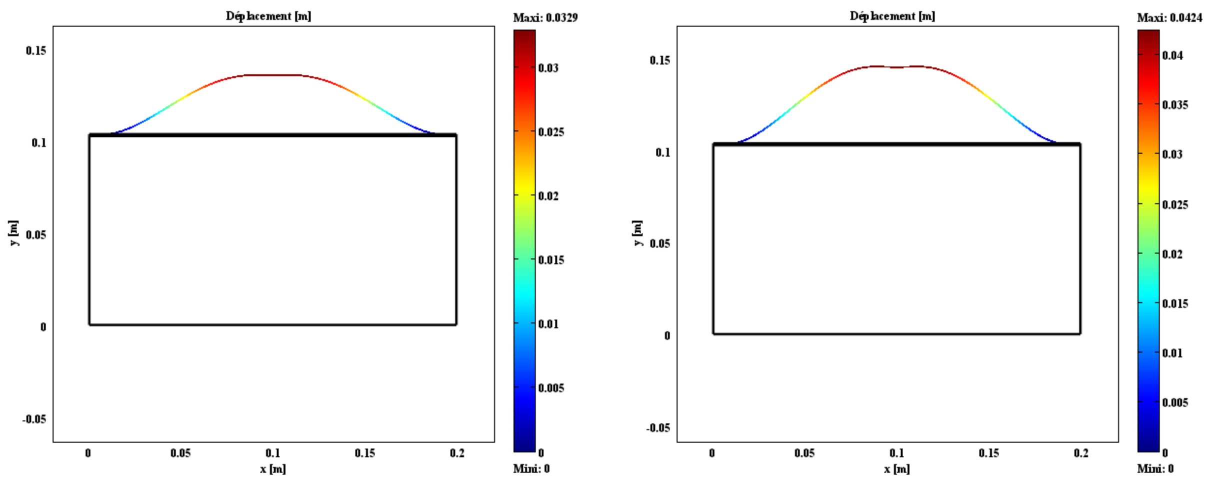

(*e*) (*f*)

Fig. 4. Deformed Shape of Aluminium Sheet under Increasing Static Pressures: (*a*) $\boldsymbol{P = 10^4\ Pa}$; (*b*) $\boldsymbol{P = 2 \times 10^4\ Pa}$; (*c*) $\boldsymbol{P = 4 \times 10^4\ Pa}$; (*d*) $\boldsymbol{P = 6 \times 10^4\ Pa}$; (*e*) $\boldsymbol{P = 8 \times 10^4\ Pa}$; (*f*) $\boldsymbol{P = 10^5\ Pa}$;

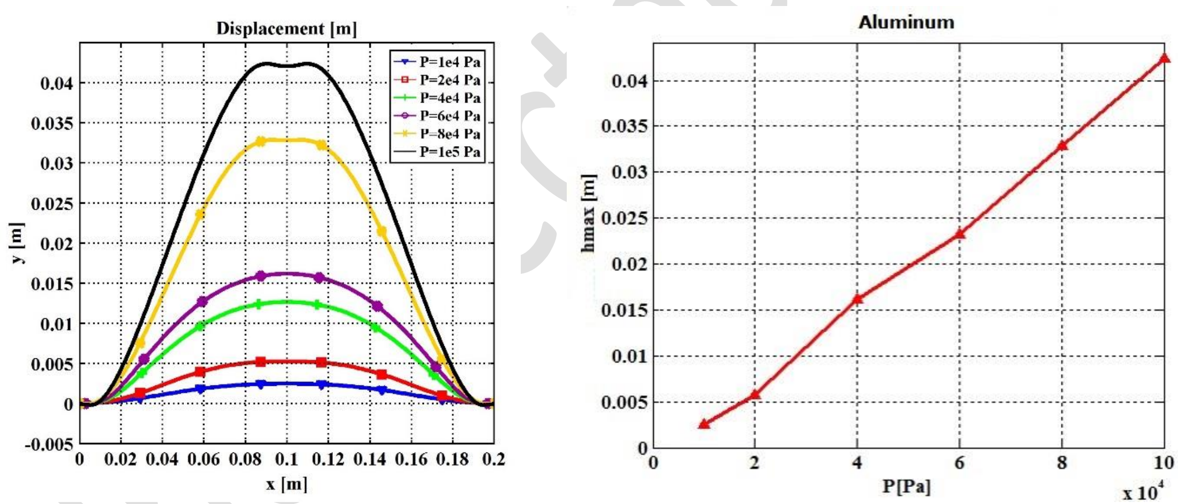

(*a*) (*b*)

Fig. 5. (*a*) Overlay of Deformed Mid-Lines of the Aluminum Sheet for all Pressure Levels; (*b*) Maximum Central Displacement as a Function of Applied Pressure

The relationship is essentially linear over the entire range, with a slope of approximately $3.5\ mm$ per $10^4\ Pa$. This linearity indicates that the sheet remains within the elastic regime for all pressure levels

10.22060/EEJ.2026.25813.6014

considered and that the static-pressure idealization captures the essential load–deformation behavior without the need for a fully coupled fluid model.

3-2- Comparative Deformation Response of Aluminum, Copper, and Steel

To assess the influence of material stiffness on EHF response, free-forming simulations were repeated for copper and structural steel using the same geometry, mesh, and pressure range as for aluminum (see Section 3.1). The resulting deformed shapes for copper are shown in Fig. 6, and for steel in Fig. 7.

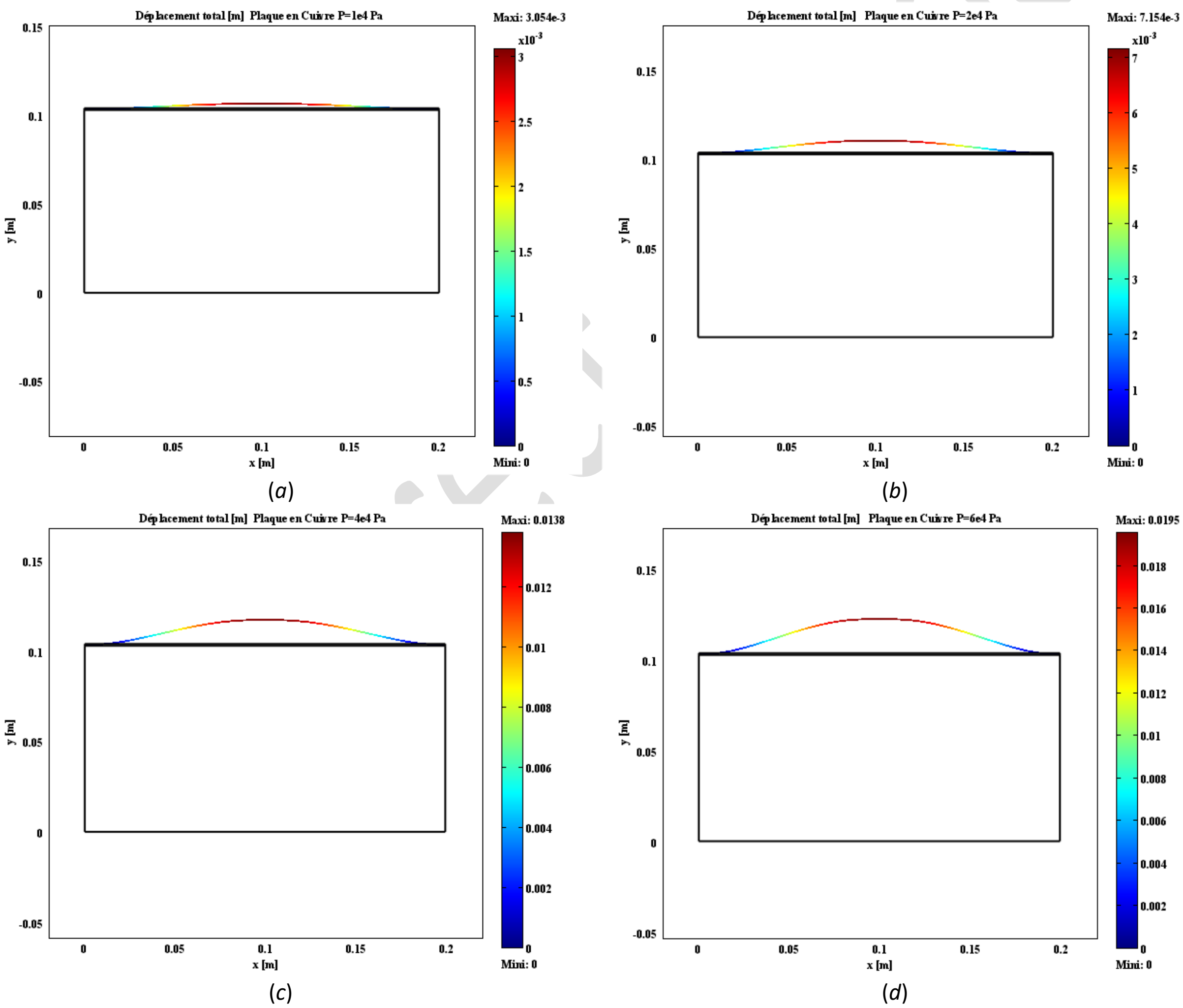

10.22060/EEJ.2026.25813.6014

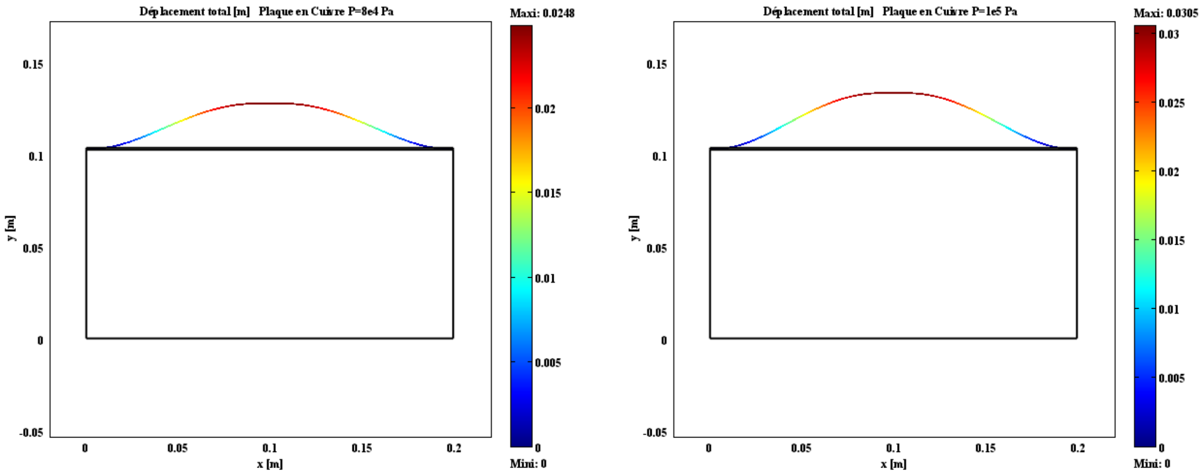

(*e*) (*f*)

Fig. 6. Deformed Shape of Copper Sheet under Increasing Static Pressures: (*a*) $\boldsymbol{P = 10^4\ Pa}$; (*b*) $\boldsymbol{P = 2 \times 10^4\ Pa}$; (*c*) $\boldsymbol{P = 4 \times 10^4\ Pa}$; (*d*) $\boldsymbol{P = 6 \times 10^4\ Pa}$; (*e*) $\boldsymbol{P = 8 \times 10^4\ Pa}$; (*f*) $\boldsymbol{P = 10^5\ Pa}$;

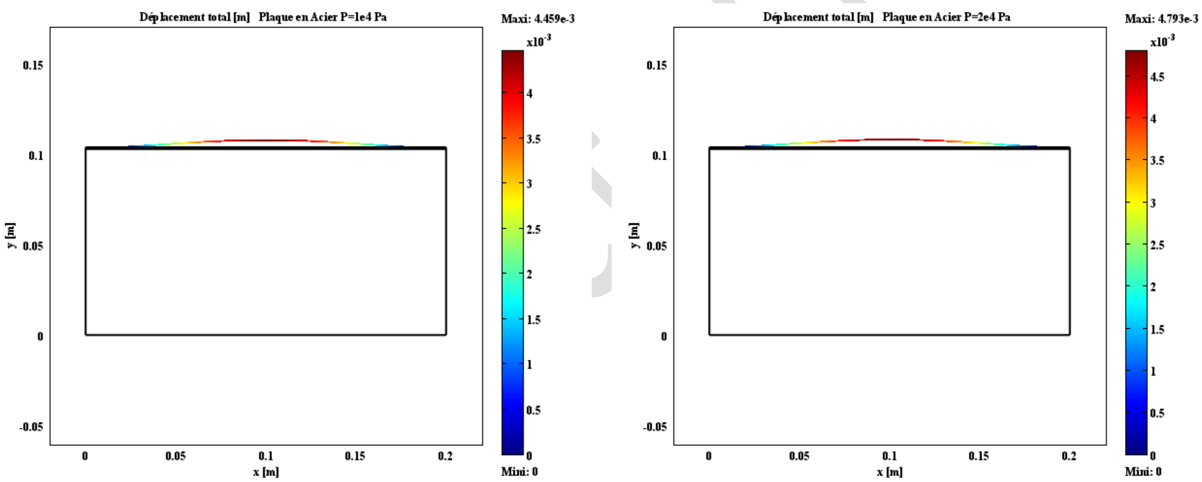

(*a*) (*b*)

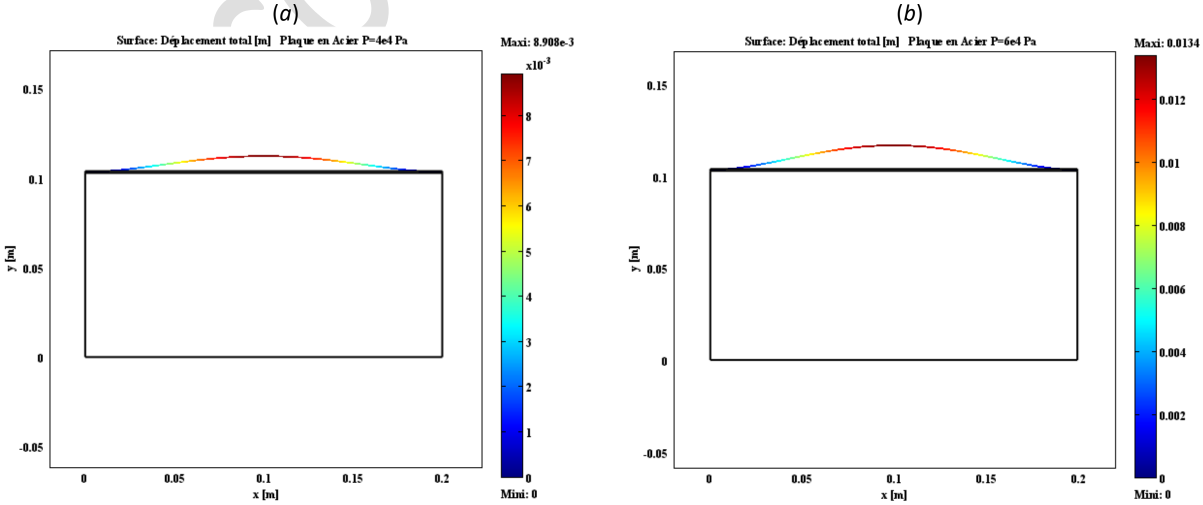

10.22060/EEJ.2026.25813.6014

(*c*) (*d*)

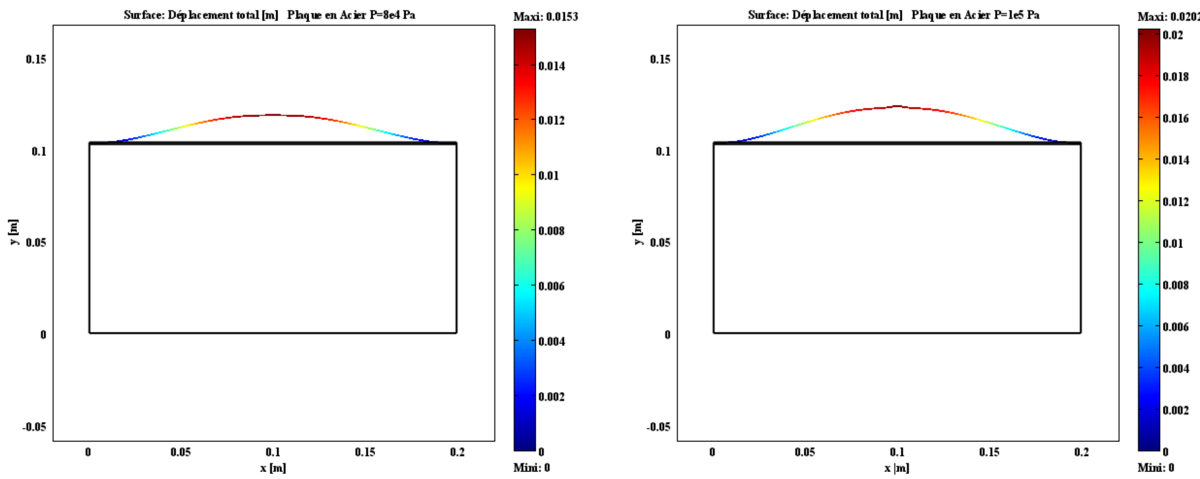

(*e*) (*f*)

Fig. 7. Deformed Shape of Structural Steel Sheet under Increasing Static Pressures: (*a*) $\boldsymbol{P = 10^4\ Pa}$; (*b*) $\boldsymbol{P = 2 \times 10^4\ Pa}$; (*c*) $\boldsymbol{P = 4 \times 10^4\ Pa}$; (*d*) $\boldsymbol{P = 6 \times 10^4\ Pa}$; (*e*) $\boldsymbol{P = 8 \times 10^4\ Pa}$; (*f*) $\boldsymbol{P = 10^5\ Pa}$;

Qualitatively, the copper and steel blanks deformed into smooth, symmetric domes similar to aluminum, but with markedly smaller amplitudes for the same pressure level. At $10^4\ Pa$, the central deflections of all three materials were negligible. At intermediate pressures, the differences became noticeable: at $4 \times 10^4\ Pa$, for example, aluminium reached roughly $14\ mm$, copper roughly $11\ mm$, and steel only about $8\ mm$. The maximum vertical displacements for copper and steel are plotted against the applied pressure in Fig. 8. For copper, the displacement–pressure relationship is nearly perfectly linear over the entire range, reaching approximately $30\ mm$ at $10^5\ Pa$. For structural steel, the trend is also increasing but deviates slightly from strict linearity, especially above $6 \times 10^4\ Pa$, where the slope becomes somewhat shallower. At the highest pressure, the steel blank is displaced by roughly $20\ mm$.

10.22060/EEJ.2026.25813.6014

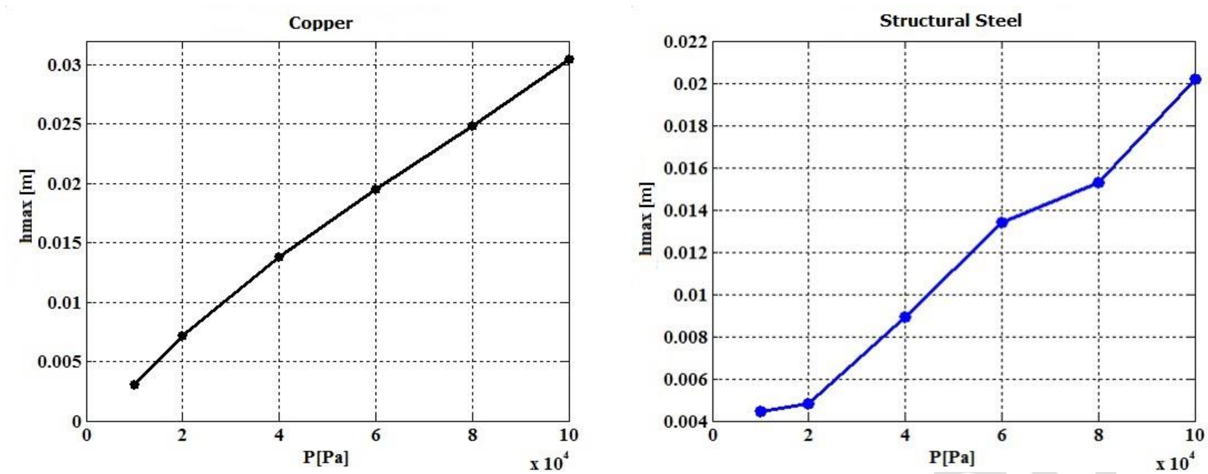

(*a*) (*b*)

Fig. 8. Maximum Central Displacement as a Function of Applied Pressure for (*a*) Copper; (*b*) Structural Steel

The direct comparison of the three materials at the maximum pressure $P = 10^5\ Pa$ is presented in Fig. 9, where the deformed mid-lines are overlaid. The ranking is unequivocal: aluminum exhibits the largest central deflection ($\approx 42\ mm$), followed by copper ($\approx 30\ mm$), and steel ($\approx 20\ mm$). This order is exactly inverse to the Young's modulus of the materials: aluminium (70), copper (110), and steel (200). The purely elastic model, therefore, predicts that the elastic deformation response under identical pressure loading is controlled primarily by the elastic stiffness, with the most compliant material deforming the most.

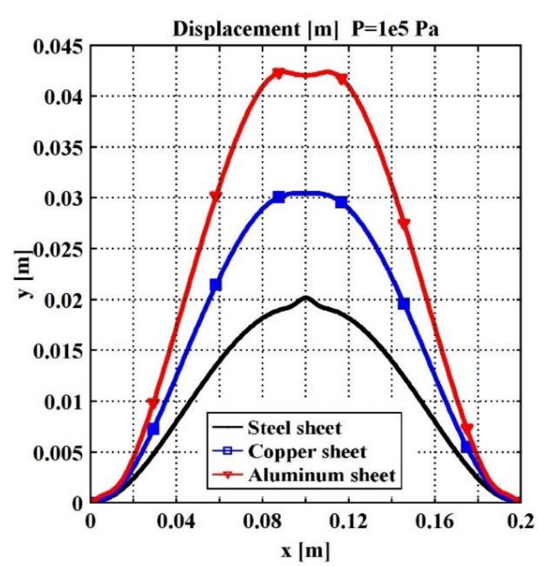

10.22060/EEJ.2026.25813.6014

Fig. 9. Overlay of Deformed Mid-Lines of Aluminium, Copper, and Structural Steel at $\boldsymbol{P = 10^5\ Pa}$

It is important to emphasize that these results reflect elastic compliance, that is, the structural stiffness of the blank, rather than plastic formability in the manufacturing sense. A complete assessment of formability would require incorporating plasticity, strain hardening, and strain-rate effects, which are not included in the present simplified model.

The observed behavior is consistent with the experimental findings of Melander *et al.* [14], who noted that lower-strength, lower-modulus materials tend to exhibit larger bulging heights in EHF free forming. The linearity obtained for copper and aluminum confirms that, within the elastic approximation, the static-pressure model can rank the relative elastic compliance of different metals without the need for pressure- or material-specific calibration. This ranking provides a useful stiffness-based indicator for material selection in EHF applications.

However, the slightly non-proportional response of steel suggests that its higher stiffness may bring the sheet closer to the transition where geometric nonlinearities become non-negligible, even within an elastic framework. In reality, plastic yielding would further amplify the differences, as aluminum and copper yield at lower stresses than steel, reducing their effective stiffness more rapidly beyond the elastic limit. The present elastic comparison, despite its simplicity, already provides a useful qualitative and, to a large extent, quantitative guide for initial material screening in EHF applications, based on the relative elastic compliance of the candidate materials. However, for accurate prediction of permanent deformation and forming limits, a more comprehensive model accounting for plasticity and strain-rate effects would be required.

It is important to clarify that in the context of the present linear-elastic model, the deflection results reflect the structural compliance of the sheet blank, i.e., the elastic deformation response under the applied pressure, rather than the plastic formability (permanent deformation capacity) typically considered in manufacturing. Plasticity, strain hardening, and strain-rate sensitivity, all of which are known to

10.22060/EEJ.2026.25813.6014

significantly influence the forming limits of metals under high-speed conditions (e.g., [10,18]), are not accounted for in the current formulation. Consequently, the material ranking presented here should be interpreted as a stiffness-based elastic compliance ranking rather than a definitive assessment of plastic formability. Nevertheless, this ranking provides a useful first-order indicator for material selection and die-filling feasibility, as the elastic stiffness governs the initial deformation response and the ability of the sheet to conform to die geometries under the applied pressure pulse. Future work incorporating plasticity and strain-rate-dependent material models will enable a more comprehensive formability evaluation.

3-3- EHF Die Forming Accuracy

The second series of simulations addressed the forming of sheets into rigid dies, thereby assessing the ability of the static-pressure model to predict die-filling accuracy. Two die geometries were investigated: a conical die and a truncated-conical die, both corresponding to the experimental programme of Melander *et al.* [14]. Aluminum and copper blanks were loaded with constant pressures of $6 \times 10^4\ Pa$ and $7 \times 10^4\ Pa$, respectively. The dies were modelled as fixed rigid boundaries; contact was assumed frictionless and enforced through a penalty method. The deformed profiles obtained with the conical die are shown in Fig. 10*a* for copper at $7 \times 10^4\ Pa$ and Fig. 10*b* for aluminum at $6 \times 10^4\ Pa$. In both cases, the sheet assumed the overall V-shape of the die, but a clear departure from perfect conformity was observed at the apex.

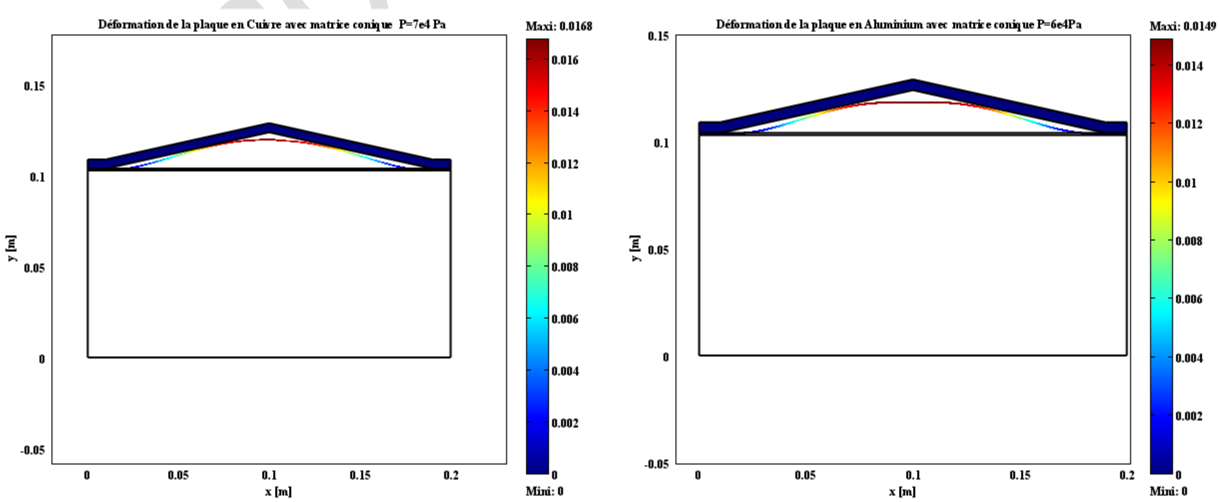

10.22060/EEJ.2026.25813.6014

(*a*) (*b*)

Fig. 10. Conical Die-Based Deformed Shape of (*a*) Copper; (*b*) Aluminium

The material did not fully penetrate the sharp tip of the cone; instead, a rounded profile with a finite radius persisted, indicating that the purely elastic sheet cannot locally match the discontinuous die curvature under the applied static pressure. The gap between the sheet and the die apex was visibly larger for copper than for aluminum, consistent with the higher stiffness of copper.

The results for the truncated-conical die are displayed in Fig. 11*a* for copper at $7 \times 10^4\ Pa$ and Fig. 11*b* for aluminum at $6 \times 10^4\ Pa$. With the sharp apex removed, the conformity improved appreciably: the sheet followed the sloped side walls and the flat bottom more closely. Nevertheless, small but measurable gaps remained along the side walls and at the transitions between the inclined and horizontal die parts.

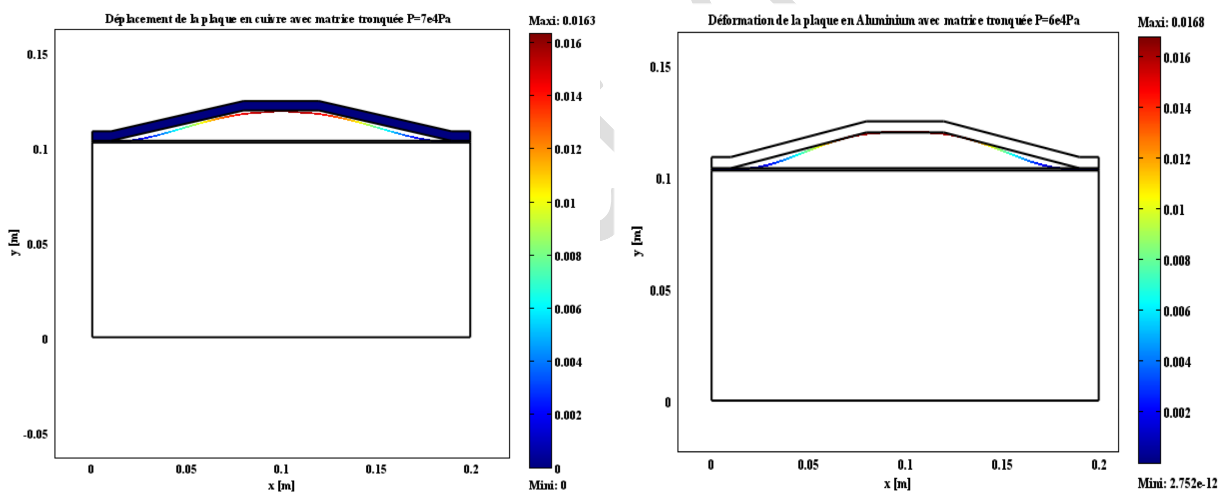

(*a*) (*b*)

Fig. 11. Truncated-Conical Die-Based Deformed Shape of (*a*) Copper; (*b*) Aluminum

These numerical observations are in qualitative and quantitative agreement with the experimental measurements reported by Melander *et al.* [14]. In their study, the vertical distance between the formed sheet and the die surface was systematically recorded for different steel grades (see Fig. 12).

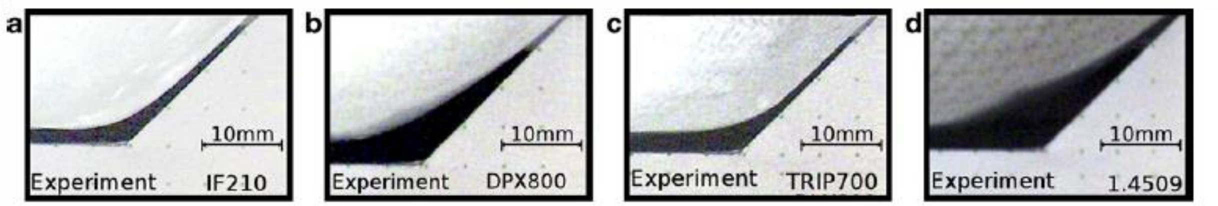

Fig. 12. Experimentally Measured Vertical Distances between the Formed Sheet and the Die Surface for Different Steels [14]

3-4- Time Evolution of Sheet Deformation under Sinusoidal Pressure Pulse

To evaluate the dynamic response of the sheet within the simplified static-pressure framework, a transient simulation was carried out on the aluminum blank in the free-forming configuration. Instead of a constant pressure, a single half-sinusoidal pulse was applied to the central loaded segment:

$$P(t) = P_{max} \sin\left(\frac{\pi t}{T}\right) \qquad 0 \leq t \leq T \tag{15}$$

with a peak amplitude $P_{max} = 10^5\ Pa$ and a pulse duration $T = 100\ \mu s$, representative of the impulse delivered by a typical EHF discharge. The transient solver integrated the equations of motion (see Eq. (1)) using a constant time step, and the vertical displacement at the center of the sheet was recorded as a function of time.

The applied pressure history is shown in Fig. 13a. It rises smoothly from zero to its maximum at $t = \frac{T}{2} = 50\ \mu s$ and returns to zero at $t = T$. The corresponding time evolution of the central deflection is displayed in Fig. 13b. The displacement closely follows the temporal shape of the pressure pulse, reaching a peak value of approximately $35\ mm$ near $t = 50\ \mu s$, i.e., at the instant of maximum pressure. A slight phase lag of a few microseconds is visible, which reflects the inertial resistance of the sheet material. Even though the material model is purely elastic, the mass term in Eq. (1) introduces a finite acceleration time. After the pressure returns to zero, the sheet undergoes a damped elastic recovery (the oscillations visible in the tail of the curve are numerical artefacts of the undamped elastic model and would be attenuated if structural damping were included).

10.22060/EEJ.2026.25813.6014

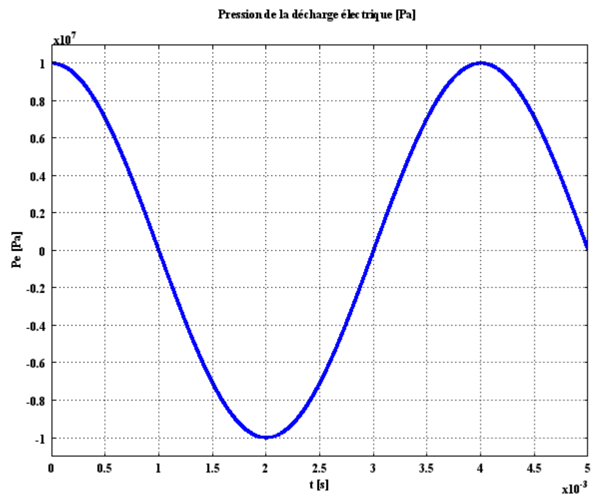

(*a*)

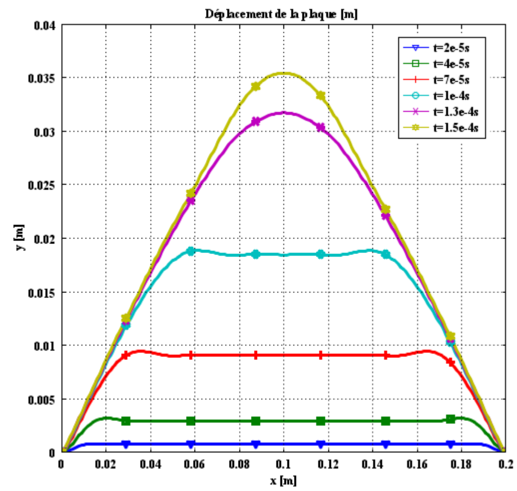

(*b*)

Fig. 13. (*a*) Sinusoidal Pressure Pulse Applied to Aluminum Sheet; (*b*) Time Evolution of the Central Displacement

These results confirm that the static-pressure idealization, when embedded in a transient solver, is capable of capturing the essential features of the dynamic EHF event. The computationally inexpensive transient analysis can therefore be used to study the influence of pulse shape and duration on the forming outcome without resorting to a fully coupled fluid–structure simulation.

3-5- Discussion and Remarks

In this Section, we discuss the numerical results obtained from various applications, along with a comparative analysis against findings from relevant studies in the literature. We also present the main limitations of the current model and outline future research directions to improve its predictive capabilities.

3-5-1 Comparative Analysis and Validation with State-of-the-art Approaches

The present numerical framework is compared with the EHF model developed by Melander *et al.* [14]. Both studies investigate free forming and die forming of sheet metals under electrohydraulic loading. However, significant differences exist in the numerical formulation and material description. Melander *et al.* employed an explicit finite-element formulation in *ABAQUS*, explicitly representing the water chamber and the propagation of a pressure wave generated by the electrical discharge. In addition, the sheet material

10.22060/EEJ.2026.25813.6014

was described using an *elastoplastic Johnson–Cook constitutive model* calibrated from tensile tests over a wide range of strain rates. Their simulations were validated quantitatively against experimental dome heights, strain distributions, and die-filling accuracy. In contrast, the present study adopts a simplified two-dimensional pressure-driven formulation implemented in COMSOL Multiphysics. An equivalent pressure applied to a localized region of the sheet replaces the complex electrohydraulic discharge and fluid–structure interaction. To contextualize the present results within the broader research landscape, Table 2 summarizes the key findings of this study alongside relevant experimental and numerical data from the literature.

Table 2. Comparison of the Present Results with Literature Data

Model	**Material**	**Loading Condition**	**Max Displacement $[mm]$**
	14509 Steel		33
Melander *et al.* [14]	DPX800 Steel	$10^5\ Pa$	35
	TRIP700 Steel		45
	Steel		20
Our Model	Aluminum	$10^5\ Pa$	42
	Copper		30

As shown in Table 2, the present results are in close agreement with those reported by Melander *et al.* [14]. The larger displacements predicted for aluminum (42 mm) and copper (30 mm) reflect the lower elastic modulus of these materials, consistent with the stiffness-based ranking expected under identical loading conditions.

Moreover, Table 3 provides a comprehensive summary comparison between the present model and the approach of Melander *et al.* [14], highlighting the key differences in numerical formulation, material behavior, and computational cost.

Table 3. Comprehensive Comparison of the Present Model with the Framework of Melander *et al.* [14]

Criterion	**Our Model**	**Melander *et al.* [14] Model**
Forming Process	EHF	EHF

10.22060/EEJ.2026.25813.6014

Main Objective	Develop a simplified pressure-driven numerical framework for free and die EHF and compare the deformation response of different metals	Investigate numerically and experimentally EHF free forming and die forming of sheet steels
Numerical Software	COMSOL Multiphysics	ABAQUS
Approach	Simplified pressure-driven FEM	Explicit FEM
Pressure Loading	Equivalent pressure applied to the formed sheet	Pressure wave propagated through water
Materials	Aluminum, Copper and Steel	DPX800, TRIP700 and 14509 Steels
Material Behavior	Linear elastic	Elastoplastic
Max Deformation	20mm for Steel, 30mm for Copper, and 42mm for Aluminum	33mm for 14509 Steel, 35mm for DPX800 Steel, and 45mm for TRIP700 Steel
Computational Cost	Low (Suitable for Parametric studies)	High
Free Forming	Investigated	Investigated
Die Forming	Conical and truncated-conical dies	Truncated-conical die
Strength	Simple, low computational cost, and easy parametric analysis	Plasticity and experimental validation
Limitation	Linear elasticity	High computational cost and simplified pressure-wave assumptions
Contributions	Efficient pressure-based framework for different materials using EHF	EHF model for steel sheet

The comparison in Table 3 reveals that while Melander *et al.* [14] employed a more complex and computationally expensive model incorporating plasticity and explicit fluid–structure interaction, the present simplified approach achieves comparable accuracy in predicting macroscopic deformation trends at a fraction of the computational cost. This makes the present framework particularly suitable for rapid parametric studies and initial material screening in industrial applications. Both models confirm that the deformation response is primarily governed by the peak pressure magnitude and the material stiffness, supporting the validity of the static-pressure idealization for macroscopic deformation prediction.

Indeed, the numerical results show that a simplified finite element model, where the electrohydraulic shockwave is represented by a uniform static pressure applied over a small central area, can successfully reproduce the key features of free and die forming of sheet metals. The predicted displacements, the linear

10.22060/EEJ.2026.25813.6014

pressure–deformation trends for aluminum and copper, the material formability ranking, and the incomplete die filling observed in conical dies all agree well with the experimental findings of Melander *et al.* [14], supporting the assumption that sheet deformation is governed mainly by peak pressure and blank stiffness rather than detailed fluid dynamics. Physically, the short EHF pressure pulse causes the sheet to respond in an almost quasi-static manner, meaning equivalent static loads can accurately predict maximum deformation while greatly reducing computational cost.

3-5-2 Limitations of the Current Model

However, the model has important limitations: it assumes purely linear elastic material behavior, neglects fluid–structure interaction and shockwave propagation effects, and is restricted to two-dimensional plane stress conditions, limiting accuracy for large plastic deformation, local pressure variations, and complex three-dimensional geometries. Even so, the approach remains highly valuable for industrial applications because it can be solved rapidly on standard computers, enabling efficient parametric studies of pressure, electrode position, and die geometry, while reducing the need for costly experimental trials and guiding the setup of more advanced simulations.

A further important limitation concerns the *kinematic assumptions of the model*. The strain-displacement relationships (see Section 2.2.2) are based on the small-deformation (linear) approximation, which assumes infinitesimally small displacements relative to the sheet dimensions. However, the maximum central deflection of approximately 35 mm on a 1 mm thick sheet yields a deflection-to-thickness ratio of 35, well beyond the validity range of linear kinematics. Consequently, geometric nonlinearity effects, such as membrane stiffening, are not captured by the current formulation. The quantitative displacement values, particularly at higher pressures, should therefore be interpreted with caution; the results are qualitatively indicative of material compliance trends rather than quantitatively exact predictions of absolute deformation.

3-5-3 Future Research Directions

While the present study focused on *Aluminum*, *Copper*, and *Structural Steel*, future work will extend the methodology to include additional lightweight materials, such as magnesium alloys and advanced high-strength steels, which are of increasing interest in automotive lightweighting. Furthermore, the current 2D plane-stress model will be expanded to a full 3D formulation to better capture complex die geometries, asymmetric deformation patterns, and local pressure variations. The incorporation of plasticity and strain-rate-dependent constitutive models is also planned to enable more accurate predictions of permanent deformation and fracture limits. Additionally, emerging hybrid forming trends, such as the combination of electrohydraulic and electromagnetic processes, warrant further numerical and experimental investigation to fully exploit the potential of *high-speed forming technologies* (e.g., [22-25]).

4. Conclusions

In this paper, we have presented a numerical investigation of EHF of sheet metals using a simplified finite-element model implemented in COMSOL Multiphysics. The model replaces the complex multiphysics of the underwater electrical discharge with an equivalent static pressure applied at the center of the sheet, an approach validated in previous experimental studies. The research examined free forming of three engineering metals, aluminum, copper, and structural steel, across a wide range of pressure levels, as well as die forming into conical and truncated-conical dies, and a time-dependent analysis under a sinusoidal pressure pulse. The parametric study confirmed a nearly linear pressure–displacement relationship for all three materials, with aluminum exhibiting the largest deformation ($\sim 42mm$), followed by copper ($\sim 30\ mm$) and steel ($\sim 20\ mm$), consistent with their elastic compliance. These results reflect the relative stiffness of the materials rather than their plastic formability. While the simplified elastic model provides a useful stiffness-based ranking for material screening, a complete formability assessment would require incorporating plasticity, strain hardening, and strain-rate effects. Die-forming simulations reproduced the residual gaps measured experimentally, confirming the model's ability to predict

10.22060/EEJ.2026.25813.6014

macroscopic die-filling accuracy. The time-dependent analysis under a sinusoidal pulse captured the dynamic response with only a slight inertial lag.

References

[1] I. Boutana, M.R. Mekideche, "Finite Element Model Analyzing Dynamical Behavior of Sheet Electromagnetic Forming". In: *6th IEEE International Multi-Conference on Systems, Signals and Devices*, pp. 1-6, 2009. Doi: https://doi.org/10.1109/SSD.2009.4956684

[2] H. Bali, I. Hafsaoui, B. Makhlouf, "A Simultaneous Resolution Method for Coupling Field_Circuit Equations for Steady-State Skin Effect Problems". In: *2018 IEEE International Conference on Electrical Sciences and Technologies in Maghreb*, pp. 1-6, 2018. Doi: https://doi.org/10.1109/CISTEM.2018.8613543

[3] I. Boutana, M.R. Mekideche, O. Cheriet, O. Kouissem, "A Coupled Finite Element Analysis and Parametric Study of Tube Forming by Electromagnetic Compression and Expansion". *Applied Physics A*, vol. 132, no. 7, art. 645, 2026. Doi: https://doi.org/10.1007/s00339-026-09819-1

[4] I. Boutana, M.R. Mekideche, "Exploring Electromagnetic Tube Expansion Based on Field Concentrator: An Analytical Model and Numerical Study". *Journal of Microwaves, Optoelectronics and Electromagnetic Applications*, vol. 23, no. 4, art. e2024280065, 2024. Doi: https://doi.org/10.1590/2179-10742024v23i4280065

[5] I. Boutana, A. Bousba, Y.N. Benhadj, "Numerical Modeling of Industrial Parts Manufacturing using Electromagnetic Hemming Process". *The International Journal of Advanced Manufacturing Technology*, vol. 133, no. 3, pp. 1943-1959, 2024. Doi: https://doi.org/10.1007/s00170-024-13869-1

[6] I. Boutana, "Advanced Numerical Modeling of Electrohydraulic Sheet Metal Formability". In: *3rd International Conference on Mechatronics and Automation Technology*, pp. 345-351, 2024. Doi: https://doi.org/10.3233/ATDE241261

[7] I. Boutana, M.R. Mekideche, B. Benalia, S. Achouche, "Advancing Sheet Metal Formability: An In-Depth Numerical Investigation and Enhanced Modeling of Electrohydraulic Process". In: *11th World Congress on Electrical Engineering, Computer Systems and Science*, art. 103, 2025. Doi: https://doi.org/10.11159/eee25.103

[8] M. Seth, V.J. Vohnout, G.S. Daehn, "Formability of Steel Sheet in High Velocity Impact". *Journal of Materials Processing Technology*, vol. 168, no. 3, pp. 390-400, 2005. Doi: https://doi.org/10.1016/j.jmatprotec.2004.08.032

[9] A. Rohatgi, E.V. Stephens, R.W. Davies, M.T. Smith, A. Soulami, S. Ahzi, "Electro-Hydraulic Forming of Sheet Metals: Free-Forming vs. Conical-Die Forming". *Journal of Materials Processing Technology*, vol. 212, no. 5, pp. 1070-1079, 2012. Doi: https://doi.org/10.1016/j.jmatprotec.2011.12.014

[10] V.S. Balanethiram, G.S. Daehn, "Hyperplasticity: Increased Forming Limits at High Workpiece Velocity", *Scripta Metallurgica et Materialia*, vol. 30, no. 4, 1994. Doi: https://doi.org/10.1016/0956-716X(94)90613-0

[11] A.V. Mamutov, S.F. Golovashchenko, J.J. Bonnen, A.J. Gillard, S.A. Dawson, L. Maison, "Electrohydraulic Forming of Light Weight Automotive Panels". In: *7th International Conference on High Speed Forming*, pp. 115-124, 2016

[12] I. Boutana, M.R. Mekideche, "A Multiphysics Framework for Investigating Electromagnetic Pulse Joining of Multi-Material Assemblies". *Journal of the Brazilian Society of Mechanical Sciences and Engineering*, vol. 48, no. 9, art. 655, 2026. Doi: https://doi.org/10.1007/s40430-026-06610-4

[13] A.V. Mamutov, S.F. Golovashchenko, V.S. Mamutov, J.J. Bonnen, "Modeling of Electrohydraulic Forming of Sheet Metal Parts". *Journal of Materials Processing Technology*, vol. 219, pp. 84-100, 2015. Doi: https://doi.org/10.1016/j.jmatprotec.2014.11.045

[14] A. Melander, A. Delic, A. Björkblad, P. Juntunen, L. Samek, L. Vadillo, "Modelling of Electro Hydraulic Free and Die Forming of Sheet Steels". *International Journal of Material Forming*, vol. 6, no. 2, pp. 223-231, 2013. Doi: https://doi.org/10.1007/s12289-011-1080-5

[15] Y. Ledoux, "Experimental Investigation of the Pulse Duration on the Efficiency and Electrode Wear of Electrohydraulic Forming Process", *Manufacturing Review*, vol. 10, art. 17, 2023.

[16] A. Ali, M. Ahmed, S. Kumar, M. Soni, K.S. Gavel, V. Chilla, "Effect of Bridge Wire Material in Electro-Hydraulic Forming of AA5754 Sheet Metal". *Canadian Metallurgical Quarterly*, vol. 65, no. 1, pp. 960-974, 2026. Doi: https://doi.org/10.1080/00084433.2025.2471615

[17] A.V. Mamutov, S.F. Golovashchenko, N.M. Bessonov, V.S. Mamutov, "Electrohydraulic Forming of Low Volume and Prototype Parts: Process Design and Practical Examples", *Journal of Manufacturing and Materials Processing*, vol. 5, no. 2, art. 47, 2021. Doi: https://doi.org/10.3390/jmmp5020047

[18] S.F. Golovashchenko, A.J. Gillard, A.V. Mamutov. "Formability of Dual Phase Steels in Electrohydraulic Forming", *Journal of Materials Processing Technology*, vol. 213, no. 7, pp. 1191-1212, 2013. Doi: https://doi.org/10.1016/j.jmatprotec.2013.01.026

[19] G.W. Milton, J.R. Willis, "On Modifications of Newton's Second Law and Linear Continuum Elastodynamics". *Proceedings of the Royal Society A: Mathematical, Physical and Engineering Sciences*, vol. 463, no. 2079, pp. 855-880, 2007

[20] C.R. Doering, J.D. Gibbon, "*Applied Analysis of the Navier-Stokes Equations*". Cambridge University Press, 1995

[21] Q. Zhang, T. Hisada, "Studies of the Strong Coupling and Weak Coupling Methods in FSI Analysis". *International Journal for Numerical Methods in Engineering*, vol. 60, no. 12, pp. 2013-2029, 2004. Doi: https://doi.org/10.1002/nme.1034

[22] I. Boutana, M.R. Mekideche, "Numerical Investigation of Thickness-Driven Formability in High-Speed Electromagnetic Sheet Forming". In: *2nd IEEE International Conference on Electronic Engineering and Information Systems*, pp. 1-5, 2025. Doi: https://doi.org/10.1109/EEISS65394.2025.11085721

[23] I. Boutana, "A Numerical Investigation and Process Optimization of Magnetic Pulse Welding for Similar and Dissimilar Materials". *Continuum Mechanics and Thermodynamics*, vol. 37, no. 5, art. 76, 2025. Doi: https://doi.org/10.1007/s00161-025-01409-5

[24] I. Boutana, O. Cheriet, O. Kouissem, "Innovative Numerical Analysis of Electromagnetic Tube Compression for Lightweight Material Applications". In: *1st IEEE International Conference on Mechanical and Electrical Engineering for Green Energy Technologies*, pp. 1-5, 2025. Doi: https://doi.org/10.1109/MEEGET65999.2025.11512259

[25] I. Boutana, M.R. Mekideche, O. Boultif, A. Zait, "Next-Generation Printed Circuit Boards Manufacturing: An Innovative Numerical Investigation using Electroforming Process". *The International Journal of Advanced Manufacturing Technology*, vol. 137, no. 7, 4169-4180, 2025. Doi: https://doi.org/10.1007/s00170-025-15412-2